# Directional results and absolute archaeointensity determination by the classical Thellier and the multi-specimen DSC protocols for two kilns excavated at Osterietta, Italy

Evdokia Tema, Pierre Camps, Enzo Ferrara, Thierry Poidras

# Directional results and absolute archaeointensity determination by the classical Thellier and the MSP-DSC protocols for two kilns excavated at Osterietta, Italy

Tema, E.[1], Camps, P.[2], Ferrara, E.[3], Poidras, T.[2]

[1] *Dipartimento di Scienze della Terra, Università degli Studi di Torino, via Valperga 35, 10125, Torino, Italy, evdokia.tema@unito.it*

[2] *Géosciences Montpellier, CNRS and Université Montpellier 2, Montpellier, France*

[3] *Istituto Nazionale di Ricerca Metrologica, Strada delle Cacce 91, I-10135 Torino, Italy*

**Abstract**

We present a detailed rock-magnetic and archaeomagnetic study of two brick kilns (named OSA and OSB) discovered at the location of Osterietta, in Northern Italy. The magnetic properties of representative samples have been investigated to identify the nature of the magnetic carriers, their domain state and thermal stability, and investigate their suitability for archaeomagnetic determinations. Thermally stable, mainly pseudo-single (PSD) domain magnetite is identified as the main magnetic carrier. The full geomagnetic field vector has been determined for the two kilns, including directional and intensity analysis. Archaeointensities have been recovered with both the classical Thellier and the multi-specimen protocols. The multi-specimen procedure was performed with a very fast-heating oven developed at Montpellier. A Matlab code for anisotropy correction during the Thellier experiment is provided. The archaeointensity results obtained from both techniques for OSA kiln are of high quality and in good agreement between them, while for the OSB kiln Thellier results are characterized by large standard deviation and the MSP technique

was not successful. The obtained full geomagnetic field vector (declination, inclination and intensity) has been used for the archaeomagnetic dating of the two structures suggesting that the OSA kiln was for last time used between 1761-1841 AD and the OSB kiln between 1752-1831 AD, at 95 % of probability. This study shows that intensity determinations do not restrict the dating results when referring to the last few centuries, as this period is characterized by very small intensity variations.

*Keywords:* Secular variation; geomagnetic field vector; archaeomagnetic dating; Italy

## 1. Introduction

Baked clay archaeological materials often contain small quantities of ferromagnetic minerals that under certain conditions can register the direction and intensity of the Earth's magnetic field in the past. When heated at high temperatures, baked clay archaeological materials, such as kilns, hearths, bricks and pottery lose their magnetization and while cooling, they acquire a thermoremanent magnetization (TRM) that has the characteristics (direction and intensity) of the ambient magnetic field that is usually the Earth’s magnetic field. Unless the material gets subsequently reheated or chemically altered, the TRM acquired remains stored in the archaeological artefacts and can be nowadays experimentally recovered offering important information about the past variations of the Earth's magnetic field.

In the case that the age of the studied archaeological artefacts is well known based on the stratigraphy, archaeological findings and/or independent absolute dating methods such as radiocarbon, thermoluminescence, or dendrochronology, the obtained archaeomagnetic data can be used as reference points to draw regional

secular variation (SV) curves and to improve the global geomagnetic field models. When no precise dating is available, the archaeomagnetic direction and intensity obtained experimentally can be used for dating the last firing of the studied material after comparison with reference SV curves.

During the last decade, several archaeomagnetic studies (e.g. Schnepp and Lanos, 2006; Gómez-Paccard and Beamud, 2008; Tema and Lanza, 2008; Tema, 2013; Tema et al., 2014) have shown that archaeomagnetism can be a valuable dating tool for archaeology, particularly for the areas where a detailed SV curve is available and where no organic material for radiocarbon dating has been found. However, most of the up to now available studies are based on the determination of the direction of the Earth's magnetic field and only few of them include also archaeointensity analysis (Jordanova et al., 2004; Casas et al., 2007; Herries et al., 2008; De Marco et al., 2008; Tema et al., 2013), most probably because of its more complicated experimental determination.

In this paper, we present a detailed rock-magnetic and archaeomagnetic study of two rescue excavation kilns discovered at the location of Osterietta, in Northern Italy. The full geomagnetic field vector has been determined and the archaeointensity for each kiln has been obtained with both the classical Thellier (Thellier and Thellier, 1959) and the multi-specimen protocols (Biggin and Poidras, 2006; Dekkers and Böhnel, 2006; Fabian and Leonhardt, 2010). A Matlab code for anisotropy correction during the Thellier experiment is provided and the archaeointensity results obtained from the Thellier and multi-specimen methods are compared and discussed. The full geomagnetic field vector has been used for archaeomagnetic dating of the two kilns after comparison with the reference curves produced by the SCHA.DIF.3K European geomagnetic field model (Pavón-Carrasco et al., 2009).

## 2. Archaeological site and sampling

The two studied kilns were discovered in 2010, during the works for the expansion of the Alessandria's ring road, at the location of Osterietta (44.9º N, 8.6º E), in Northern Italy (Fig. 1). During two excavation campaigns that took place in 2010 and 2011, a production workshop has been identified and three kilns (in the areas 3, 4 and 6) have been excavated (Venturino et al., 2013). For the present archaeomagnetic study, samples have been collected from two of the kilns, namely OSA (area 3) and OSB (area 6), situated around 1 km away from the fortification walls of the old Alessandria city, known as *Cittadella of Alessandria* (Fig. 2a).

OSA is a big kiln, oriented N-S, and consists of 6 *praefurnia* tunnels constructed by bricks (Fig. 2b). It has been only partly excavated as the combustion chamber is probably extended towards the northern part of the kiln, situated nowadays under the nearby highway. Each *preafurnia* tunnel is invested by series of bricks, horizontally situated. The combustion chamber, even though not excavated, was probably rectangular, as big as the excavated front of the kiln. The baking floor was constructed by bricks, pieces of which have been found in the refilling material.

OSB kiln is situated around 100 m west of the OSA kiln and is oriented W-E. It is heavily damaged because of the intensive later agriculture activities in the area. It is not well conserved and most of the bricks that covered the *preafurnia* and the combustion chamber are lost. However, it has characteristics similar to those of OSA kiln, even though with smaller dimensions. There are still clearly visible two *preafurnia* tunnels of dimensions 2.5x0.9 m (however the total number of the tunnels is not known) and the rests of two support and baking floors (Fig. 2c).

No ceramics or other characteristic artefacts have been found in the filling of the structures. The lack of such objects that could offer dating information and the kilns' common architecture style makes it hard for archaeologists to constrain the time of the use and the abandonment of this large production workshop. The only available dating information is based on a preliminary thermoluminescence (TL) analysis made on two bricks from kiln OSA, that suggests an age not older than XVI-XVII centuries AD (Venturino et al., 2013). However, the very limited amount of material sampled at the initial phase of the excavation (July 2010) for TL analysis has not allowed a complete and detailed TL investigation (Raimondo Prosperi, ARKAIA, personal communication). Furthermore, the proposed TL date has been calculated only from the total absorbed TL dose without including measurements of the environmental and annual dose, and the corresponding corrections. The available TL date can thus be used only as a general reference and does not offer a precise dating.

For archaeomagnetic analysis, a total of 15 brick hand samples from OSA kiln have been collected (Fig. 2b), coming from the three first tunnels (numbered 1 to 6 from East to West). From OSB kiln, 8 brick hand samples have been collected from the *preafurnia* tunnels (Fig. 2c). All collected samples were oriented *in situ* with a magnetic compass and an inclinometer, signing the orientation arrow directly on the bricks' surface. No consolidation at the laboratory was needed as the bricks were very compact and well conserved. Bad weather conditions prevented the use of a sun compass. From each independently oriented brick, at least four cylindrical specimens of standard dimensions (diameter = 25.4 mm, height = 22 mm) were drilled in the laboratory. The prepared specimens were used for magnetic mineralogy experiments and for the determination of the archaeomagnetic direction and intensity.

## 3. Magnetic mineralogy

The magnetic properties of the collected bricks have been investigated to identify the nature of the magnetic carriers, their domain state behaviour and their thermal stability with the objective to check their suitability for archaeomagnetic determinations. Isothermal remanent magnetization (IRM) acquisition curves, thermal demagnetization of three-axes IRM components (Lowrie, 1990), hysteresis loops and low-field thermomagnetic curves were measured for pilot samples.

IRM acquisition curves of representative samples were obtained at the ALP Palaeomagnetic laboratory (Peveragno, Italy) with an ASC pulse magnetizer to impart the IRM, applying stepwise increasing magnetic fields up to 1.6 T, and a JR6 spinner magnetometer (Agico) to measure the remanent magnetization. The obtained curves for both OSA and OSB kilns are very similar, with a saturation of the magnetization reached at low fields varying from 0.2 to 0.4 T (Fig. 3). This observation is consistent with the presence of a low-coercivity mineral such as magnetite. Such interpretation is further supported by the thermal demagnetization experiments of a three component IRM (Lowrie, 1990). A composite orthogonally induced IRM was imparted to representative samples: first a maximum field (1.6 T) was applied along the cylinder – axis (Z), then an intermediate field (0.5 T) along the Y-axis and finally a minimum field (0.1 T) along the X-axis. Stepwise thermal demagnetization results of the three-axes IRM (Fig. 4) show the dominance of the magnetically soft fraction (< 0.1 T); however, in some samples mainly from OSB kiln (Fig. 4 c,d) the medium coercivity component is also important while the high coercivity component is in all cases negligible.

Hysteresis measurements were performed with a Lake Shore 7400 Vibrating Sample Magnetometer (VSM) equipped with a chamber for low temperature (liquid

151 nitrogen) measurement at INRIM (Torino, Italy). Five samples from the OSA kiln
152 have been analysed. The hysteresis curves obtained at room temperature for
153 representative samples (OSA-3, OSA-16 and OSA-19) show the coexistence of
154 different magnetic contributions (Fig. 5a). The analysed powders exhibit, in fact, a
155 ferrimagnetic behaviour, as appreciable from the hysteresis loops appearing at low
156 field values (coercive field $H_c$ value ~ 10 mT) along with paramagnetic contributions.
157 For further investigation of the ferrimagnetic carriers, hysteresis loops have been
158 corrected for the paramagnetic contribution (Fig. 5 a, b, c). The shape of the loops and
159 the low value of the coercive field suggest the presence of a soft magnetic phase, such
160 as magnetite. Figs. 5b and 5c show the changes with temperature of the magnetization
161 cycles exhibited by samples OSA-4 and OSA-7, respectively, in the temperature
162 range from - 196 °C to 25 °C. From the graphs, a significant content of ferromagnetic
163 pseudo-single domain particles can be appreciated, which is related to the hysteretic
164 behaviour and maintained at all the applied temperatures. The change of the shape of
165 the hysteresis curves with temperature observed in figures 5b and 5c is expected to
166 depend on the presence of smaller particles that progressively unblock their
167 magnetization contribution moving from the soft ferrimagnetic to the
168 superparamagnetic state as temperature decreases (see Figs 5b and 5c). Although
169 variable, the superparamagnetic contribution of OSA samples is relevant: in the case
170 of OSA-7 (Fig. 5c) there is a gain of magnetization higher than 50 % in the passage
171 from 25 °C to - 196 °C.

172 Weak-field magnetic susceptibility measurements as a function of temperature
173 (K–T curves) were carried out at the Palaeomagnetic laboratory of Géosciences
174 Montpellier (France). Pieces of archaeological material from representative samples
175 were first crushed and sieved to collect the 0.4-0.8 mm size fraction. Then K–T

curves were acquired by heating the material from the liquid nitrogen temperature (-196 °C) obtained with a cryostat apparatus (CS-L) to a high-temperature (around 620 °C) obtained with a CS-3 furnace coupled to the KLY-3 Kappabridge instrument (Agico, Czech Republic) and then cooled down to room temperature. K-T experiments indicate negligible magnetochemical changes for all samples (Fig. 6) as attested by the reversible shape of the heating and the cooling branches. The Curie temperatures, generally spreading between 550 and 580 °C, are indicative of the presence of magnetite or Ti-magnetite, in agreement with the results obtained from IRM and hysteresis experiments. We interpret the progressive increase in the susceptibility below the Curie temperature observed for all samples from OSB as a Hopkinson peak. This effect could be caused by the rotation of magnetic moments of single-domain grains. At low temperatures, a weak Vervey transition superposed on increasing curves is also observed for samples from OSB. This observation confirms that the magnetic carrier is magnetite and could also suggest the presence of a small fraction of larger grain behaving as multi-domain. Hopkinson peaks are not clearly observed in samples from OSA. This suggests a larger size for the ferrimagnetic grains, in the PSD-like behaviour in accordance with the hysteresis results. To sum up, the K-T curves provide decisive arguments, quite encouraging for palaeointensity determinations, identifying the main remanence carrier as thermally stable SD-PSD magnetite. Note that very few samples from OSA yield a paramagnetic-like behavior (sample OSA-3b in Fig. 6). We interpret these results as a heterogeneous distribution of the scarce ferrimagnetic minerals in the baked clays.

## 4. Archaeomagnetic field vector determination

### *4.1 Archaeomagnetic direction*

One specimen per sample from the OSA and OSB kilns has been selected for the determination of the archaeomagnetic direction of each kiln. First the NRM of 15 specimens from OSA and 8 specimens from OSB was measured at the ALP Palaeomagnetic laboratory with a JR-6 spinner magnetometer. Following, all specimens have been stepwise thermally demagnetized from room temperature up to 580 $^{o}$C with a Schonstedt TSD-2 furnace. The demagnetization results are illustrated as orthogonal vector projections of the remanent magnetization (Zijderveld, 1967) (Fig. 7). Zijderveld diagrams show that the magnetic remanence is very stable and it consists of one well defined Characteristic Remanent Magnetization (ChRM) direction.

The directions of the ChRM for each specimen were evaluated from principal component analysis (Kirschvink, 1980). Directions calculated at specimen level are well defined with maximum angular deviation (MAD) generally lower than 2$^{o}$. Four specimens from OSA kiln were rejected as they didn't pass through the origin of the Zijderveld diagrams. Results from both OSA and OSB kilns at specimen level are reported in Table 1, together with the mean direction for each kiln. The statistical parameters are calculated assuming a Fisherian distribution (Fisher, 1953). Equal-area projections of the ChRM directions (Fig. 8) show a very good concentration around the mean values. The calculated mean direction for kiln OSA is: D=341.8$^{o}$, I= 66.2$^{o}$, k= 389, $\alpha_{95}$= 2.3$^{o}$ and for kiln OSB is: D= 339.6$^{o}$, I= 67.5$^{o}$, k= 504, $\alpha_{95}$= 2.5$^{o}$.

*4.2 Archaeomagnetic intensity*

*4.2.1 Experimental procedure*

Absolute intensity determinations were carried out with both the Thellier and Thellier (1959) in its classical form and the multispecimen protocols (Biggin and

Poidras, 2006; Dekkers and Böhnel, 2006; Fabian and Leonhardt, 2010). This double approach was possible as material was available in sufficient quantity. The main motivation of a double approach was to provide an additional reliability check with a multi-method consistency. All archaeointensity measurements were carried out at the Palaeomagnetic laboratory of Géosciences Montpellier.

The classical Thellier protocol was applied on 56 samples; 32 from OSA kiln and 24 from OSB. On the basis of the rock magnetic investigations carried before the palaeointensity measurements, no *a priori* sample selection was performed. The ChRMs are clearly of thermoremanent origin, not disturbed by significant secondary components, and the magnetic properties seem to be reasonably stable during the laboratory heating. The measurement protocol is as follows. The samples are heated and cooled twice at each temperature step in presence of a 50 μT induction field during cooling. The field is oriented along the cylinder axis of the core (z-axis) for the first cycle and in the opposite direction for the second one. Samples were heated in 11 steps between 120 °C and 560 °C: steps of 60 °C were applied between 120 and 300 °C, 50°C between 300 and 400 °C, 40°C between 400 and 480 °C and finally 30 °C between 480 and 540 °C. After every two-temperature steps, a pTRM check was performed to detect any alteration in the thermoremanent magnetization acquisition capacity. All heating–cooling cycles were performed in air. In our palaeointensity furnace, the temperature reproducibility between heating treatments at the same step is within 1 °C, and the intensity of laboratory field is maintained with a precision better than 0.1 μT (Camps et al., 2011). After each heating–cooling cycle, the remanent magnetization was measured with a 2G cryogenic magnetometer.

The Thellier archaeointensity measurements were corrected for magnetic anisotropy effect by means of the anisotropy of TRM (ATRM) according to a

standard procedure adopted in the Montpellier laboratory (see Fanjat et al., 2013). The ATRM tensors were determined during the Thellier experiment, at a temperature step for which at least 20% of the initial NRM is involved for the majority of samples. In this study, a temperature of 440 °C has been chosen. The samples were remagnetized at this temperature after the Thellier step (that yields +Z and – Z steps) in +X, -X, +Y, and -Y directions. All archaeointensity values were corrected for the ATRM according to Veitch et al. (1984) method. Our Matlab© code estimating this correction is provided and illustrated with a data example as supplementary material (see Appendix). Just after the ATRM tensor determination at 440 °C, the effect on the cooling rate on the acquisition of the TRM was estimated by repeating the last pTRM-check with a 4-times slower cooling rate (12 h) than the one used in the Thellier protocol (3 h). The low cooling rate is simply achieved by switching off the fans of the cooling system of our furnace during the pTRM acquisition.

The multispecimen (MSP) experiments were performed with a prototype of a very fast-heating infrared furnace developed in Montpellier (FURéMAG, patent #1256194). Two key points determine its characteristics. The first is to heat uniformly a single rock sample of a 10-cc-standard volume very fast. The second is to apply to the sample during the heating (and the cooling) a precise magnetic induction field, perfectly controlled in 3D with a measured precision better than 1° (Camps et al, in preparation). The MSP-DSC protocol (Fabian and Leonhardt 2010) was applied to both OSA and OSB kilns. As in this protocol the pTRM is imparted along the NRM direction, anisotropy correction is not necessary. During the test and the calibration of this furnace, Fanjat (2012) showed that it is also not necessary to apply cooling rate correction with the MSP protocol. The heating temperature Th is chosen freely, sufficiently high to work on a sufficient fraction of the TRM (at least 20 %) but

sufficiently low to avoid chemical alteration. From the thermal demagnetizations performed in the directional analysis, we chose for all the samples a single temperature of 400°C to impart the laboratory pTRM.

*4.2.2 Archaeointensity results*

The Thellier archaeointensity data were interpreted with the Thellier-tool software provided by Leonhardt et al. (2004). We adopted a standard set of criteria derived from those proposed by Fanjat et al. (2013) and based on the statistical parameters introduced by Coe et al. (1978) and modified by Prévot et al. (1985) to interpret each individual archaeointensity data and filter out those of poor technical quality. Archaeointensity values at specimen level are accepted when the linear segment in the Arai plots is defined by more than four points ($n > 4$) and spans over 50% of the total extrapolated ChRM. We quantified the difference between two pTRM acquisitions at the same temperature by the Difference Ratio (DRAT) parameter (Selkin and Tauxe, 2000). DRAT is expressed in percent and corresponds to the maximum difference measured between repeated pTRM acquisition normalized by the length of the selected NRM-TRM segment. A maximum acceptable threshold is fixed arbitrarily at 10 % even though for most of our accepted results is lower than 5 %/. Jointly, we checked on the directional plots computed from the archaeointensity experiments that the NRM fraction used to calculate the archaeointensity corresponds effectively to the ChRM direction of the core. For instance, the low-temperature part of the NRM may contain natural secondary magnetizations, and a spurious remanent magnetization acquired during the laboratory heating may superpose to the NRM if chemical changes in the magnetic minerals occurred. In total, 34 out of the 56

analyzed samples satisfied the quality criteria mentioned above and yielded acceptable archaeointensity determinations. The selected values at specimen level are listed in Table 2, few of them are illustrated on Figure 9. Among the 22 excluded samples, 14 are rejected because of curvature in the Arai plots in spite of a good linearity in the Zijderveld plots, 5 are rejected because of a multi-component behavior observed in the Zijderveld plot, and 3 are rejected because of a too small NRM fraction destroyed ($f \leq 0.5$) before irreversible magneto-chemical changes arise. Note that when two slopes are present in the Arai's diagrams (see for example sample OSA_7c on Figure 9), we chose the temperature interval yielding a paleointensity close to the other determinations.

Averaging the 23 acceptable results from kiln OSA, we found an archaeointensity value of 50.6 ± 2.2 μT. The individual values are fairly coherent as attested by the small value of the standard deviation (less than 5% of the average). A different case arises for kiln OSB for which a large scatter in the individual values is observed. Kiln OSB yields an archaeointensity value of 47.1 ± 6.9 μT, based on 11 acceptable results (Table 2). The large standard deviation, which is about 13% of the average, casts doubt on the reliability of this determination and it should be therefore cautiously used for archaeomagnetic dating.

The MSP archaeointensity results are processed in two steps. First, we selected "*a posteriori*" the samples for which the ratio between the fraction of NRM overprinted by the laboratory pTRM and the total NRM is between 0.2 and 0.8. This selection ensures that, if present, the multidomain pTRM-tail effect (see e.g. Dunlop and Ozdemir, 2000) will be correctly measured. In addition, only samples for which the angle between the NRM and the NRM remaining after the laboratory pTRM overprint is lower than a threshold angle here arbitrarily chosen to be 10°, have been

326 selected. This selection ensures that the NRM is the ChRM. Second, the MSP
327 archaeointensities were determined by fitting the data with robust linear regression
328 that is anchored to the point (0, -1) for the fraction and domain state corrected values
329 (see Fabian and Leonhardt, 2010, for a detailed explanation on this protocol and its
330 treatment). The robust regression is used to minimize the influence of outliers by
331 iteratively weighting the data by their distance to the fitting line (Holland and Welsh,
332 1977). We anchored the linear regression to the point (0, -1) since it represents a
333 theoretical reference: when a sample is cooled in zero field there is no pTRM
334 acquisition. We estimated the effect of the value of alpha parameter for the domain
335 state correction (Fabian and Leonhardt, 2010) by comparing the archaeointensities
336 computed for a value of 0.5 with the two archaeointensities calculated by means of
337 the two extreme values of 0.2 and 0.8.

338 MSP results are reported on Table 3 and illustrated on Figure 10. For kiln
339 OSA, on 10 samples measured, only 2 were rejected from the analysis because of a
340 low NRM fraction for the first one and significant change in direction after pTRM
341 acquisition for the second one. The eight samples selected yield a very similar
342 palaeointensity value whatever the protocol used (DB, FC, or DSC) and whatever the
343 value of alpha parameter (Table 3). As recommended by Fabian and Leonhardt
344 (2010), if not significantly different from the others, the value obtained with the MSP-
345 DSC (alpha = 0.5) has to be chosen, that is 54.5 ± 3.5 for kiln OSA. The uncertainty is
346 calculated from the regression analysis with the 95% confidence interval on the slope
347 parameter estimate. This value is in good agreement and within the error bar with the
348 value obtained with the conventional Thellier protocol.

349 For kiln OSB, it has not been possible to calculate a MSP archaeointensity
350 value. Seven out of the ten samples measured are rejected due to a too low NRM

fraction. Obviously, the set temperature of 400°C to impart a significant pTRM was a priori underestimated for a majority of samples. One can explain this mistake by a large heterogeneity in the magnetic properties of samples from kiln OSB. The remaining 3 accepted points are statistically poor: a best fitting line based on only 3 points would not be trustful.

## 5. Archaeomagnetic dating

The full geomagnetic field vector obtained for both OSA and OSB kilns has been used for archaeomagnetic dating after comparison with the reference SV curves calculated from the SCHA.DIF.3K regional geomagnetic field model (Pavón-Carrasco et al., 2009) at the site coordinates. Archaeointensity data obtained from the classical Thellier experiment, available for the two kilns have been used, even though the mean archaeointensity for OSB kiln is characterized by an important uncertainty (6.9 μT).

Possible ages at 95% confidence level have been calculated using the Matlab *archaeo_dating* tool (Pavón-Carrasco et al., 2011). The final dating for each kiln is obtained after the combination of the separate density functions for declination, inclination and intensity. For OSA, archaeomagnetic dating suggests that the kiln has been for last time used in the time interval 1761-1841 AD (Fig. 11a). If we repeat the dating using the archaeointensity value obtained by the MSP technique (54.5 ± 3.5 μT) instead of that obtained by the Thellier experiment (50.6 ± 2.2 μT), the dating result remains practically the same (1760-1841 AD). For OSB kiln, archaeomagnetic dating based on the full geomagnetic field vector suggests that it has been abandoned between 1752 and 1831 AD (Fig. 11b). Exactly the same age is obtained if dating of the OSB kiln is repeated based only on directional results. These results clearly show

that dating in the last few centuries AD is evidently controlled by the directions while archaeointensity results have almost no influence. The very small intensity variations of the Earth's magnetic field in Europe during the last five centuries (Pavón-Carrasco et al., 2009) result in the calculation of an associated too wide probability density (see intensity probability diagrams in Fig. 11) that makes dating resolution based on archaeointensity very low and therefore does not contribute to further restrict the dating results.

The dating results obtained here show that the two kilns were in use and abandoned almost contemporaneously, suggesting that they were constructed in order to satisfy the need of a large production of bricks. This dating is in good agreement with the archaeological findings of the site that suggest the presence of a big workshop at the area, with three big kilns already excavated. The hypothesis of the archaeologists that the bricks produced in the studied kilns could have been used for the construction of the fortification walls of the old city of Alessandria (Cittadella of Alessandria) is supported by our results. The Cittadella was designed by the Italian military architect Ignazio Bertola and was built between 1732 and 1808 AD, with some last parts added as late as 1833 (e.g. Magazzino del Genio) (Marotta, 1991). Its construction undoubtedly needed a large quantity of bricks and the vicinity of the kilns to the fortified walls strongly supports such connection. However, other hypothesis suggesting that the produced bricks were used for the construction of the long bridge made by stones and bricks connecting to the Cittadella, and/or for the construction between 1749 and 1831 AD of several multi-storey buildings arranged along the axis of the ancient quarter of Bergoglio, are also in good agreement with our results and cannot be excluded.

## 6. Conclusions

Two big brick kilns excavated at Osterietta provided abundant material for a detailed rock-magnetic and archaeomagnetic study. Magnetic mineralogy analysis suggested the suitability of the material for both direction and intensity determinations, indicating the presence of thermally stable, SD-PSD magnetite as the main magnetic carrier. These results encouraged the use of both classical Thellier and the multi-specimen procedures for archaeointensity determination. The main results of our study can be summarized as follows:

1. Brick samples coming from the internal part of the kilns have been heated at high temperatures and have successfully registered the direction of the Earth's magnetic field at the time of their last cooling.

2. Both classical Thellier and MSP techniques have been successfully applied to OSA kiln, giving very similar results (statistically undistinguishable).

3. For kiln OSB, even though rock-magnetic analysis showed the presence of SD-PSD thermally stable magnetite grains, both Thellier and MSP methods have not given successful results. The archaeointensity determined by the classical Thellier method shows large standard deviation, about 13% of the average, probably due to important inhomogeneities between single bricks that result in discrepancies on the archaeointensity values determined at sample level. Using the MSP protocol, it was not possible to calculate a mean archaeointensity due to the very low NRM fraction involved, probably caused by a not adequate temperature choice.

4. Archaeomagnetic dating suggests that OSA kiln was last used between 1761-1841 AD and OSB kiln between 1752-1831 AD, at 95 % of probability. In the case of both kilns, dating based on the full geomagnetic field vector gave exactly the same results with dating based only on directions. This suggests, that even when archaeointensities

are well defined with small standard deviation (as in the case of kiln OSA), intensity results do not improve the precision of archaeomagnetic dating when referring to the last few centuries. That is because of the slight variations of the intensity of the Earth's magnetic field during the last five centuries.

5. The dating results obtained here support the hypothesis that the discovered kiln workshop was used for the production of bricks during the construction of the fortified walls of the *Cittadella* of Alessandria and/or the construction of secondary walls and buildings of the ancient quarter of Bergoglio that took place between 1749 and 1831 AD.

**Acknowledgments**

We would like to warmly acknowledge the "Soprintendenza per i Beni archeologici del Piemonte e del Museo Antichità Egizie" for sampling permission. Dr. Marica Venturino, Dr. Alberto Crosetto and ARKAIA s.r.l. are particularly acknowledged for providing useful information on the excavation and fruitful discussion on the use and dating of the kilns. We are grateful to Patrick Nicol for technical help during the laboratory experiments at the Montpellier laboratory. This project was part of the PHC-Galileo program. The Géosciences Montpellier was supported by a grant from the CNRS-PNP. The FUReMAG rapid furnace construction was supported by the French National Agency for Research (ANR-12-BS06-0015). The Editor Mark Dekkers and the reviewers Harald Böhnel and Angel Carrasco are warmly acknowledged for their useful comments on the manuscript.

450

451

452

453 **References**

454

455 Biggin A. J. and Poidras T., 2006. First-order symmetry of weak-field partial
456 thermoremanence in multi-domain ferromagnetic grains. 1. Experimental evidence
457 and physical implications. *Earth and Planetary Science Letters*, 245(1-2), 438–453.
458 doi:10.1016/j.epsl.2006.02.035.

459 Camps P., Singer B., Carvallo C., Goguitchaichvili A., Fanjat G. and Allen B., 2011.
460 The Kamikatsura event and the Matuyama–Brunhes reversal recorded in lavas from
461 Tjornes peninsula, northern Iceland. *Earth Planet. Sci. Lett.,* 310, 33-44,
462 DOI:10.1016/j.epsl.2011.07.026.

463

464 Camps P., Poidras T., Fanjat G., Carvallo C. and Nicol P. Some improvements in the
465 MSP-DSC paleointensity method by means of a new type of laboratory furnace. *In*
466 *preparation for Solid Earth.*

467

468 Casas L., Linford P. and Shaw J., 2007. Archaeomagnetic dating of Dogmersfield
469 Park brick kiln (Southern England). *J. Arch. Sci.,* 34, 205-213.

470 Coe R.S., Grommé S. and Mankinen A., 1978. Geomagnetic paleointensities from
471 radiocarbon-dated lava flows on Hawai and the question of the Pacific nondipole low.
472 *J. Geophys. Res*., 83, 1740-1756.

473 Dekkers M. J. and Böhnel H. N., 2006. Reliable absolute palaeointensities
474 independent of magnetic domain state. *Earth and Planetary Science Lett*ers, 248 (1-
475 2), 508–517, DOI:10.1016/j.epsl.2006.05.040.

476 De Marco E., Spassov S., Kondopoulou D., Zananiri I. and Gerofoka E., 2008.
477 Archaeomagnetic study and dating of a Hellenistic site in Katerini (N. Greece). *Phys.*
478 *Chem. Earth*, 33, 481-495.
479
480 Dunlop D.J., and Ozdemir O., 2000. Effect of grain size and domain state on thermal
481 demagnetization tails. *Geophys. Res. Lett*., 27, 1311-1314.
482
483 Fabian K. and Leonhardt R., 2010. Multiple-specimen absolute paleointensity
484 determination: an optimal protocol including pTRM normalization, domain-state
485 correction, and alteration test. *Earth Planet. Sci. Lett*., 207, 84–94.
486 Fanjat G., 2012. Les fluctuations du champ magnétique terrestre : des variations
487 séculaires récentes aux renversements. *Available online at https://tel.archives-*
488 *ouvertes.fr/tel-00719380.*
489 Fanjat G., Camps P., Alva-Valdivia L., Sougrati M., Cuevas-Garcia M. and Perrin M.,
490 2013. First archaeointensity determinations on Maya incense burners from palenque
491 temples, Mexico : new data to constrain the Mesoamerica secular variation curve.
492 *Earth Planet. Sci. Lett*., 363, 168-180.
493
494 Fisher R.A., 1953. Dispersion on a sphere. *Proceedings of Royal Society*, London,
495 pp.295.
496
497 Gómez-Paccard M. and Beamud E., 2008. Recent achievements in archaeomagnetic
498 dating in the Iberian Peninsula: application to Roman and Mediaeval Spanish
499 structures. *J. Arch. Sci*., 35, 1389-1398.

Herries A., Kovacheva M. and Kostadinova M., 2008. Mineral magnetism and archaeomagnetic dating of a mediaeval oven from Zlatna Livada, Bulgaria. *Phys. Chem. Earth,* 33, 496-510.

Holland P.W. and Welsch R.E., 1977. Robust Regression Using Iteratively Reweighted Least-Squares. *Communications in Statistics: Theory and Methods*, A6, pp. 813–827.

Jordanova N., Kovacheva M. and Kostadinova M., 2004. Archaeomagnetic investigation and dating of Neolithic archaeological site (Kovachevo) from Bulgaria. *Phys. Earth Planet. Int*., 147, 89-102.

Kirschvink J.L., 1980. The least-square line and plane and the analysis of palaeomagnetic data. *Geophys. J. Astron. Soc*., 62, 699-718.

Leonhardt R., Heunemann C. and Krása D., 2004. Analysing absolute paleointensity determinations: acceptance criteria and the software Thelliertool4.0. *Geochem. Geophys. Geosyst.,* 5 (12), DOI:10.1029/2004GC000807.

Lowrie W., 1990. Identification of ferromagnetic minerals in a rock by coercivity and unblocking temperature properties. *Geophys. Res. Lett.*, 17, 159-162.

Marotta A., 1991. *La cittadella di Alessandria: Una fortezza per il territorio dal Settecento all'Unità*. SO.G.ED. Edizioni, Alessandria, pp. 170.

525

526 Pavón-Carrasco F. J., Osete M.L., Torta J. M. and Gaya-Piqué L. R., 2009. A regional
527 archaeomagnetic model for Europe for the last 3000 years, SCHA.DIF.3K:
528 applications to archaeomagnetic dating. *Geochem. Geophys. Geosyst.,* 10 (3),
529 Q03013, doi:10.1029/2008GC002244.

530

531 Pavón-Carrasco F.J., Rodriguez-Gonzalez J., Osete M.L. and Torta J., 2011. A Matlab
532 tool for ar-chaeomagnetic dating. *Journal of Archeological Science,* 38 (2), 408-419.

533

534 Prévot M., Mankinen E.A., Coe R.S. and Grommé C., 1985. The Steens mountain
535 (Oregon) geomagnetic polarity transition 2. Field intensity variations and discussion
536 on reversal models. *J. Geophys. Res.*, 90, 10417–10448.

537 Schnepp E. and Lanos P., 2006. A preliminary secular variation reference curve for
538 archaeomagnetic dating in Austria. *Geophys. J. Int*., 166, 91-96.

539

540 Selkin P.A. and Tauxe L., 2000. Long-term variations in palaeointensity. *Philos.*
541 *Trans. R. Soc. Lond.*, A 358, 1065-1088.

542

543 Tema E. and Lanza R., 2008. Archeaomagnetic study of a lime kiln at Bazzano
544 (Northern Italy). *Physics and Chemistry of the Earth, 33, 534-543.*

545

546 Tema E., 2013. Detailed archaeomagnetic study of a ceramic workshop at Kato
547 Achaia: New directional data and archaeomagnetic dating in Greece**.** *Bulletin of the*
548 *Geological Society of Greece,* vol. XLVII, No 3, 1279-1288.

549

550 Tema E., Fantino F., Ferrara E., Lo Giudice A., Morales J., Goguitchaichvili A.,
551 Camps P., Barello F. and Gulmini M., 2013. Combined archaeomagnetic and
552 thermoluminescence study of a brick kiln excavated at Fontanetto Po (Vercelli,
553 Northern Italy). *J. Arch. Science*, 40 (4), 2025-2035.

554

555 Tema E., Fantino F., Ferrara E., Allegretti S., Lo Giudice A., Re A., Barello F., Vella
556 S., Cirillo L. and Gulmini M., 2014. Archaeological, archaeomagnetic and
557 thermoluminescence investigation of a baked clay kiln excavated at Chieri, northern
558 Italy: contribution to the rescue of our cultural heritage. *Annals of Geophysics*, 57, 5,
559 G0548, doi: 10.4401/ag-6611.

560

561 Thellier E. and Thellier O., 1959. Sur l'intensité du champ magnétique terrestre dans
562 le passé historique et géologique, *Ann. Geophys.,* 15, 285-376.

563

564 Veitch R.J., Hedley I.G. and Wagner J.J., 1984. An investigation of the intensity of
565 the geomagnetic field during Roman times using magnetically anisotropic bricks and
566 tiles. *Arch. Sci.,* 37 (3), 359–373.

567

568 Venturino Gambari M., Crosetto A. and Prosperi R., 2013. Alessandria, località
569 Osterietta: Rinvenimento di fornaci postmedievali. *Quaderni della Soprintendenza*
570 *Archeologica del Piemonte*, 28, 187-189.

571

572 Zijderveld J., 1967. AC demagnetization of rocks: analysis of results. In: Collinson,
573 D., Creer, K., Runcorn, S. (Eds.), *Methods in Paleomagnetism*. Elsevier, New York,
574 pp. 254-256.
575
576

**Figures caption**

Fig. 1. Map of Italy with the location of the Osterietta archaeological site.

Fig. 2. a) General view of the position of the OSA and OSB kilns, situated near the the Alessandria city and its old *cittadella*. b-c) Photos and samples position of the kilns OSA and OSB, respectively.

Fig. 3. Normalized IRM acquisition curves up to 0.4 T for representative samples from a) kiln OSA and b) kiln OSB. Insets show the same IRM curves up to 1.6 T.

Fig. 4. Stepwise thermal demagnetization of three IRM components following Lowrie (1990) for representative samples from the a-b) OSA and c-d) OSB kilns. Symbols: dot= Soft- (0.1 T); diamond= Medium- (0.5 T); square= Hard- (1.6 T) coercivity component.

Fig. 5. Hysteresis loops for representative samples from OSA kiln after subtraction of the paramagnetic contribution. a) Magnetic behaviour of three different samples (OSA-3, OSA-16, and OSA-19) at room temperature; b- c) Comparison of the magnetic behavior of the same sample (sample OSA-4 and OSA-7 respectively) at different temperatures in the range -196 to 25 °C . A slight increase of the coercive field with decreasing temperature can be noticed.

Fig. 6. Dependence of weak-field susceptibility on temperature for representative samples from kilns OSA and OSB.

602

603 Fig. 7. Stepwise thermal demagnetization results from representative samples from
604 kilns OSA (upper part) and OSB (lower part) illustrated as Zijderveld plots. Symbols:
605 full dots = declination; open dots = apparent inclination.

606

607 Fig. 8. Equal area projection of the ChRM directions for kilns OSA and OSB.

608

609 Fig. 9. Composite Arai's diagrams for 2 samples from kiln OSA and 2 samples from
610 kiln OSB, respectively. Solid (open) circles are NRM-TRM points accepted (rejected)
611 to calculate the least squares line used to estimate the archaeointensity. Triangles
612 denote the pTRM checks. NRM and TRM are normalized by the NRM max and TRM
613 max, respectively.

614

615 Fig. 10. MSP archaeointensity determinations for kiln OSA (a,b) and kiln OSB (c,d),
616 respectively. Closed (open) symbols represented data used (rejected) in the robust
617 regression of the responses in Q parameters on the predictors in magnetic field (B).
618 The MSP-DB and MSP-FC data and fitting lines (a,c) are represented with magenta
619 and blue lines, respectively. For MSP-DSC plots (b,d), data and fitting lines are
620 calculated with alpha = 0.5. The dashed-black lines are the 95% confidence intervals
621 on the best fitting lines.

622

623 Fig. 11. Archaeomagnetic dating results for a) kiln OSA and b) kiln OSB. Up:
624 declination (left), inclination (middle) and intensity (right) reference secular variation
625 curves calculated from the SCHA.DIF.3K model (red curve with error band) and the
626 kiln’s measured direction and intensity (blue line with green error band); middle:

627 calculated probability density functions for declination (left), inclination (middle) and
628 intensity (right); down: combined probability density function for declination,
629 inclination and intensity.
630
631

632

633 **Tables caption**

634

635 Table 1. Archaeomagnetic directional results. Columns: Sample; Temperature interval
636 used for the calculation of the direction of the ChRM at specimen level; Declination
637 (º); Inclination (º); MAD: Maximum Angular Deviation; Mean value: N= number of
638 independently oriented samples; $D_m$= mean declination; $I_m$= mean inclination; k=
639 precision parameter; $\alpha_{95}$= 95% semi-angle of confidence according to Fisher (1953).

640

641 Table 2. Thellier-Thellier archaeointensity results.
642 Columns: n is the number of points in the interval of temperature Tmin–Tmax used
643 to determine the archaeointensities; the fraction of NRM (f), the gap factor (g), and
644 the quality factor (q) were calculated according to Coe et al. (1978); DRAT
645 corresponds to the difference ratio between repeat pTRM steps normalized by the
646 length of the selected NRM-pTRM segment; H is the uncorrected archaeointensity
647 estimate for individual specimen and uncertainty; FaTRM and FCR are the scaling
648 factors for TRM anisotropy and cooling rate corrections, respectively; unweighted
649 averages for uncorrected archaeointensities H, ATRM corrected archaeointensities
650 HaTRM, and ATRM plus cooling rate corrected archaeointensities HaTRM,CR.

651

652 Table 3. Multispecimen protocol results.
653 Archaeointensity values are estimated by the zero-crossing point of the Robust linear
654 regression on the Q parameters obtained with the MSP-DB protocol (Dekker and
655 Bohnel, 2006), fraction correction (MSP-FC) or domain state correction protocols
656 (Fabian and Leonhardt, 2010) as function of the laboratory field. The 95% confidence

interval on the archaeointensity are calculated from the 95% confidence interval on the fitting line. R-squared is the coefficient of determination indicating how well data fit the model. RMSE is the root mean squared error for the fitting line.


ÖSTERREICH
SUISSE
50 km
30 mi
© d-maps.com
Trentino-
Alto Adige
Friuli-
Venezia
Giulia
SLOVENIJA
Valle
d'Aosta
Lombardia
Veneto
Piemonte
Osterietta
(44.9° N, 8.6° E)
Liguria
Emilia-Romagna
FRANCE
Toscana
Marche
HRVATSKA
Osterietta
ITALY

Fig. 1

667

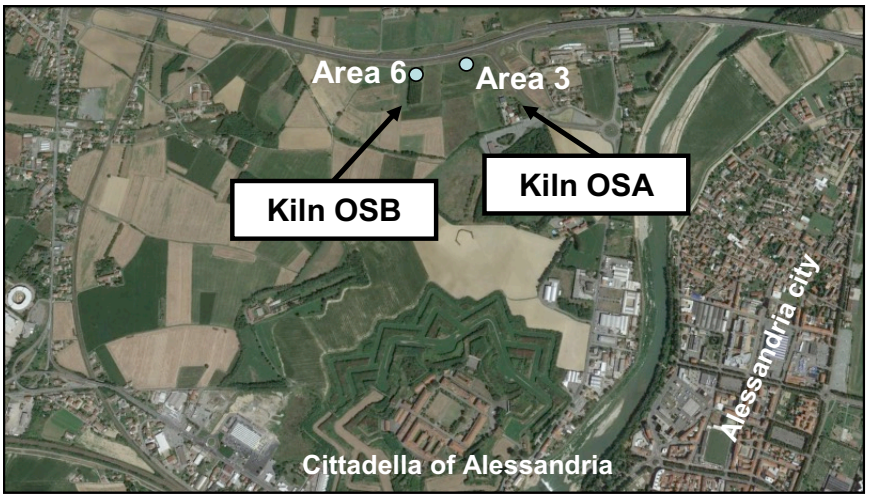


668 a)


669 b)


670 c)

671 Fig. 2

672

673

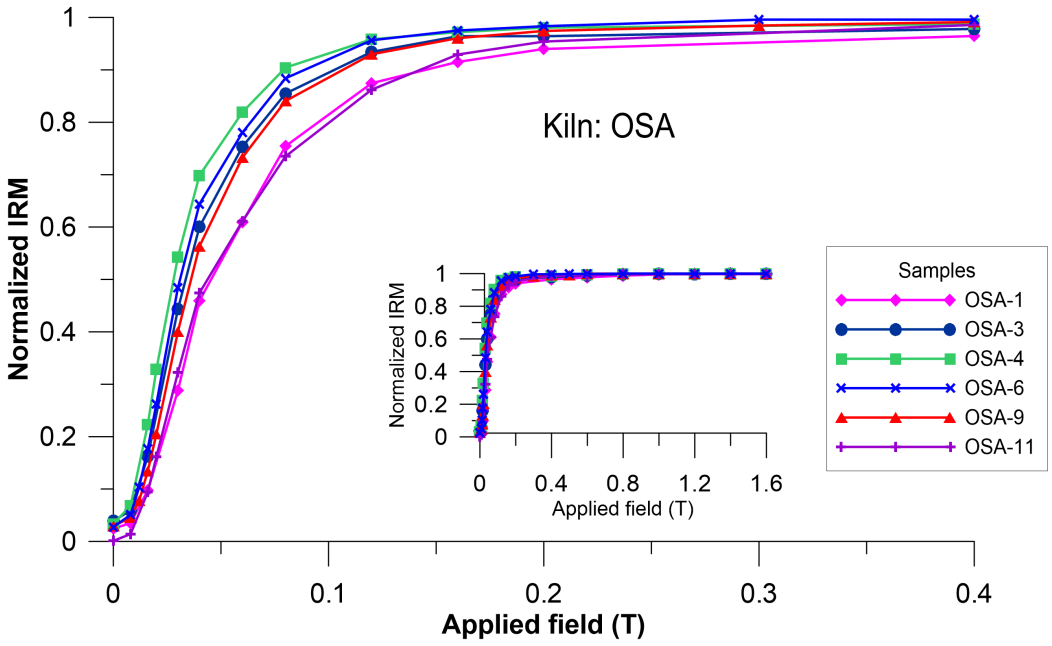
Kiln: OSA
Normalized IRM
Applied field (T)
Samples
OSA-1
OSA-3
OSA-4
OSA-6
OSA-9
OSA-11

(a)

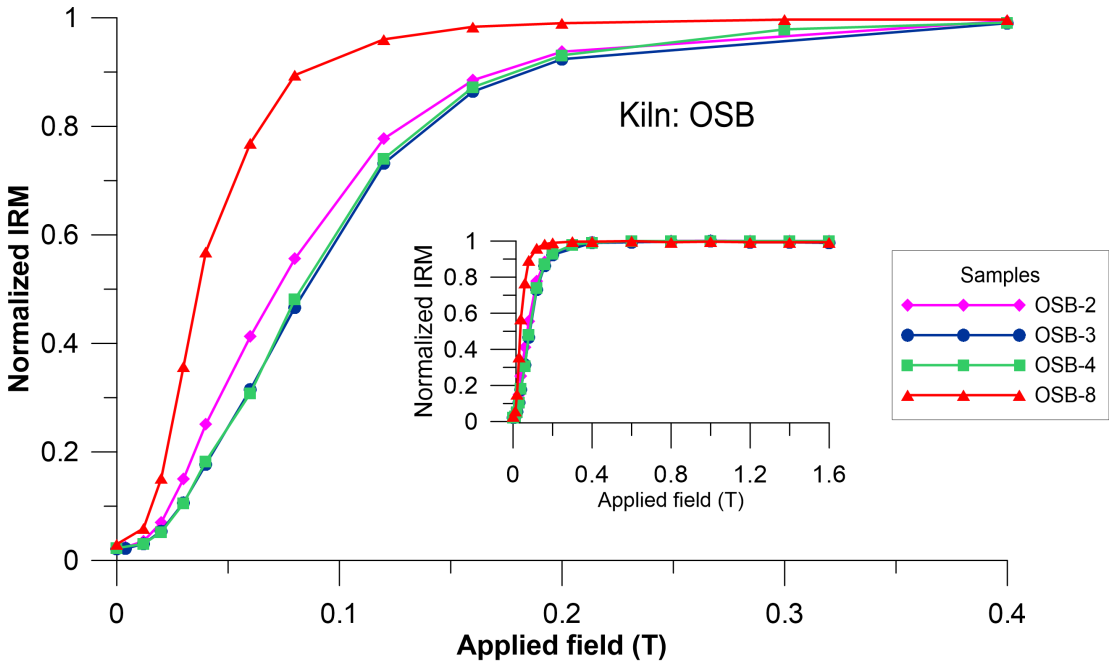
Kiln: OSB
Normalized IRM
Applied field (T)
Samples
OSB-2
OSB-3
OSB-4
OSB-8

(b)

Fig. 3

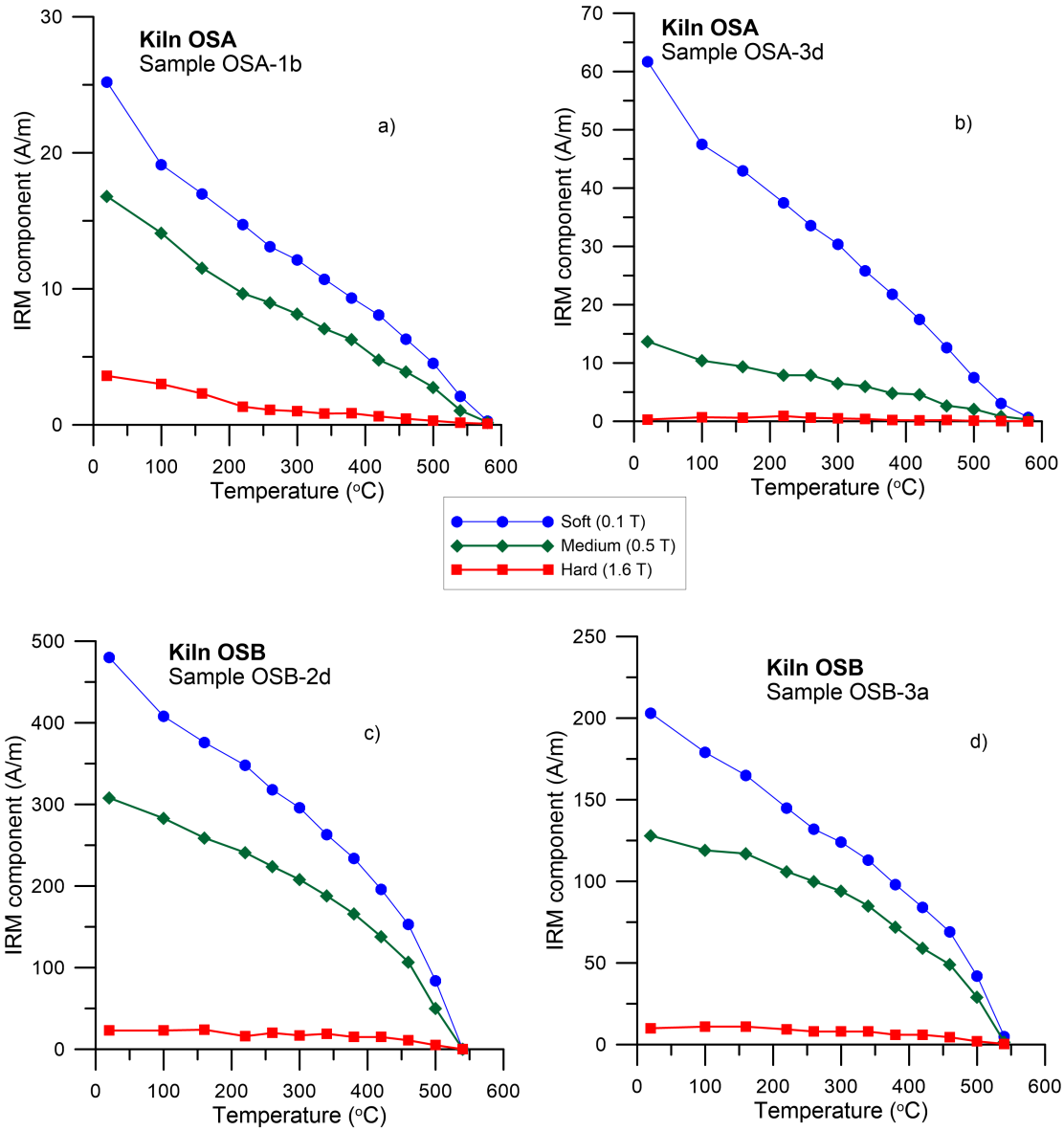
Kiln OSA
Sample OSA-1b
a)
IRM component (A/m)
Temperature (°C)
Kiln OSA
Sample OSA-3d
b)
IRM component (A/m)
Temperature (°C)
Soft (0.1 T)
Medium (0.5 T)
Hard (1.6 T)
Kiln OSB
Sample OSB-2d
c)
IRM component (A/m)
Temperature (°C)
Kiln OSB
Sample OSB-3a
d)
IRM component (A/m)
Temperature (°C)

Fig. 4

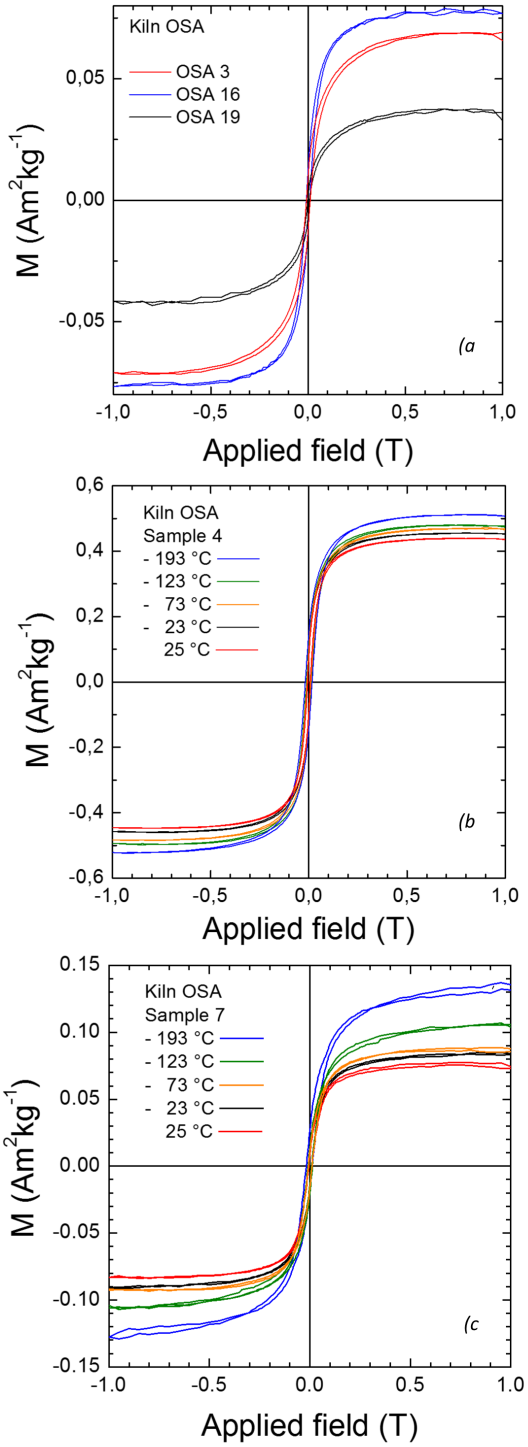


693

694 Fig. 5

695

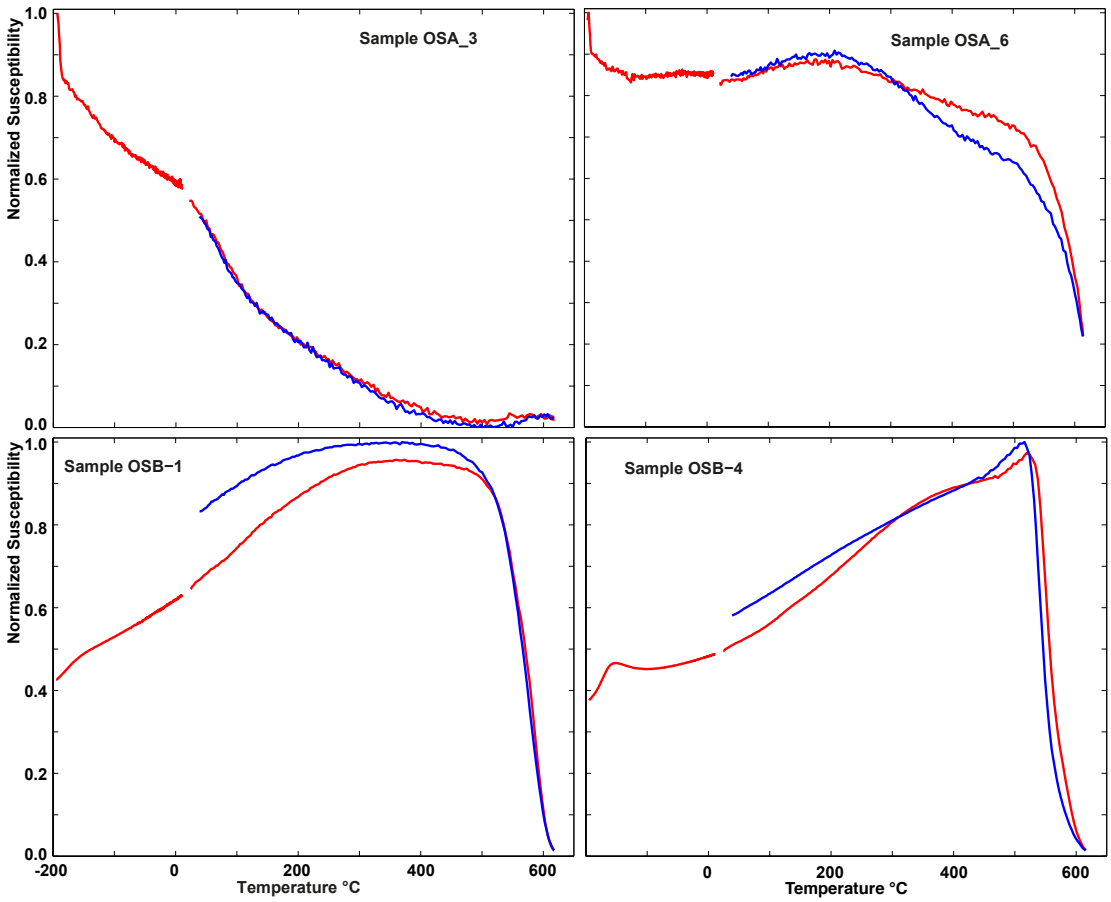
Sample OSA_3
Sample OSA_6
Sample OSB−1
Sample OSB−4
Normalized Susceptibility
Normalized Susceptibility
Temperature °C
Temperature °C
1.0
0.8
0.6
0.4
0.2
0.0
-200
0
200
400
600

Fig. 6

705

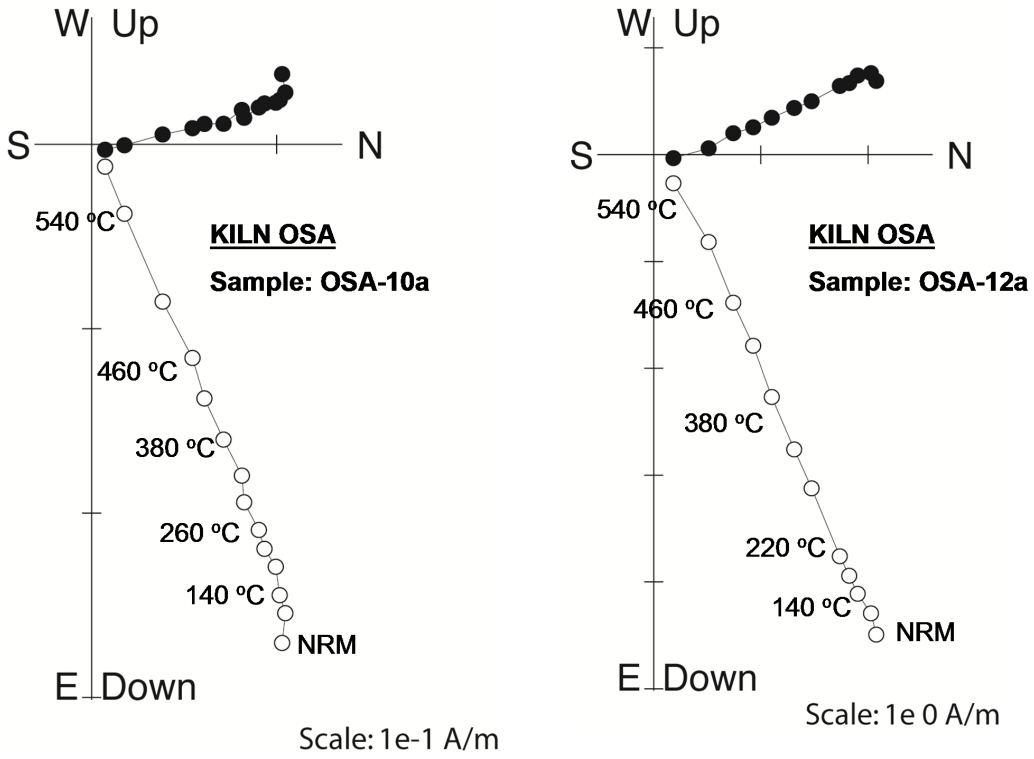


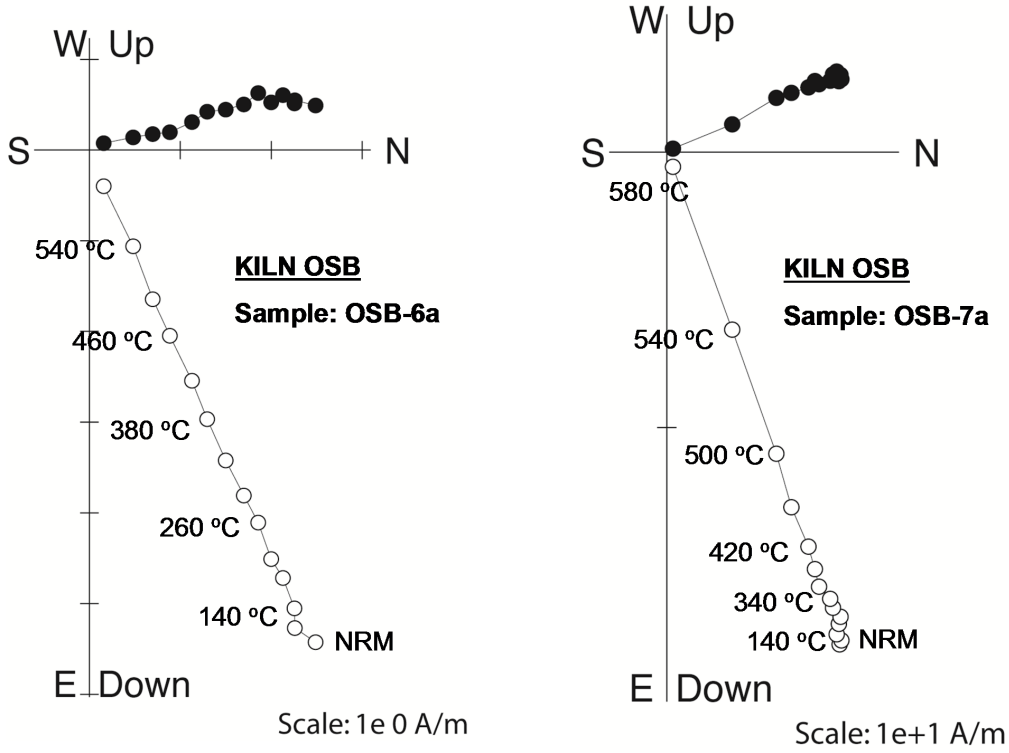


706

707

708

709 Fig. 7

710

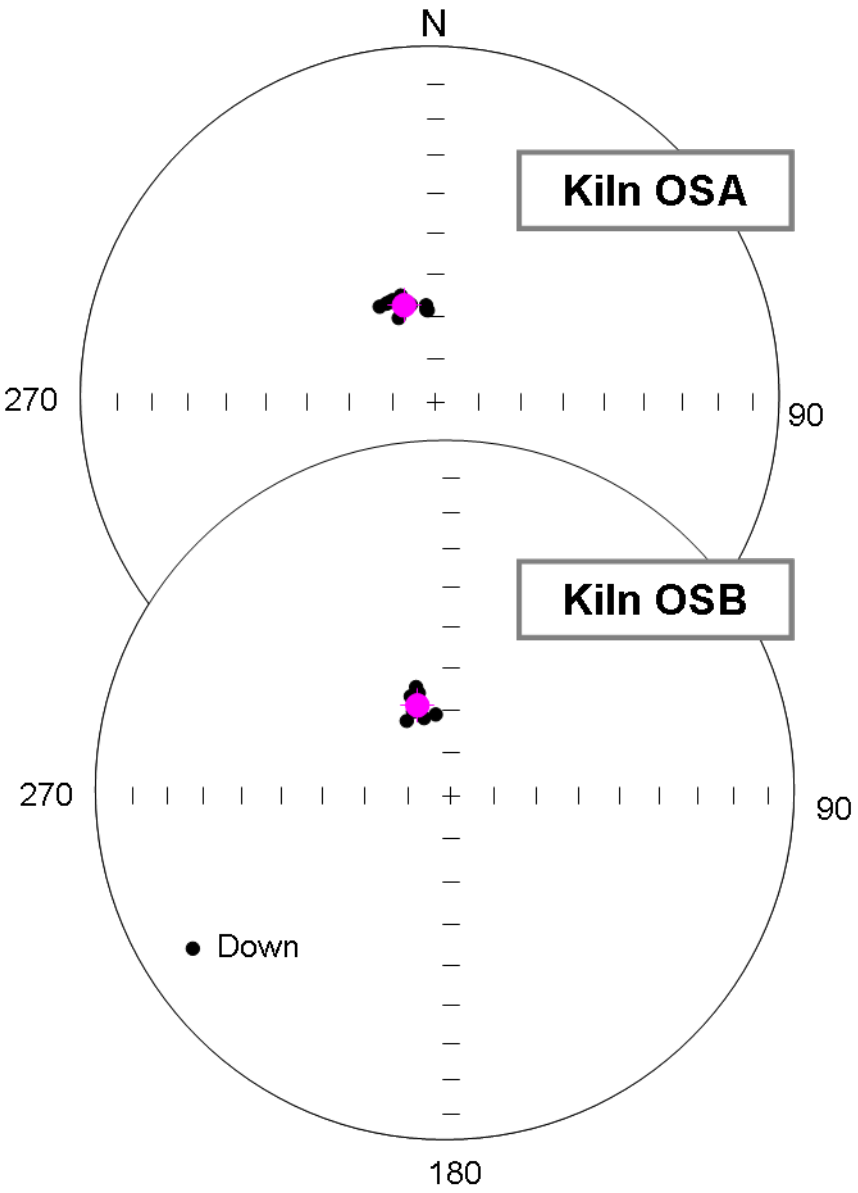


711

712

713 Fig. 8

714

715

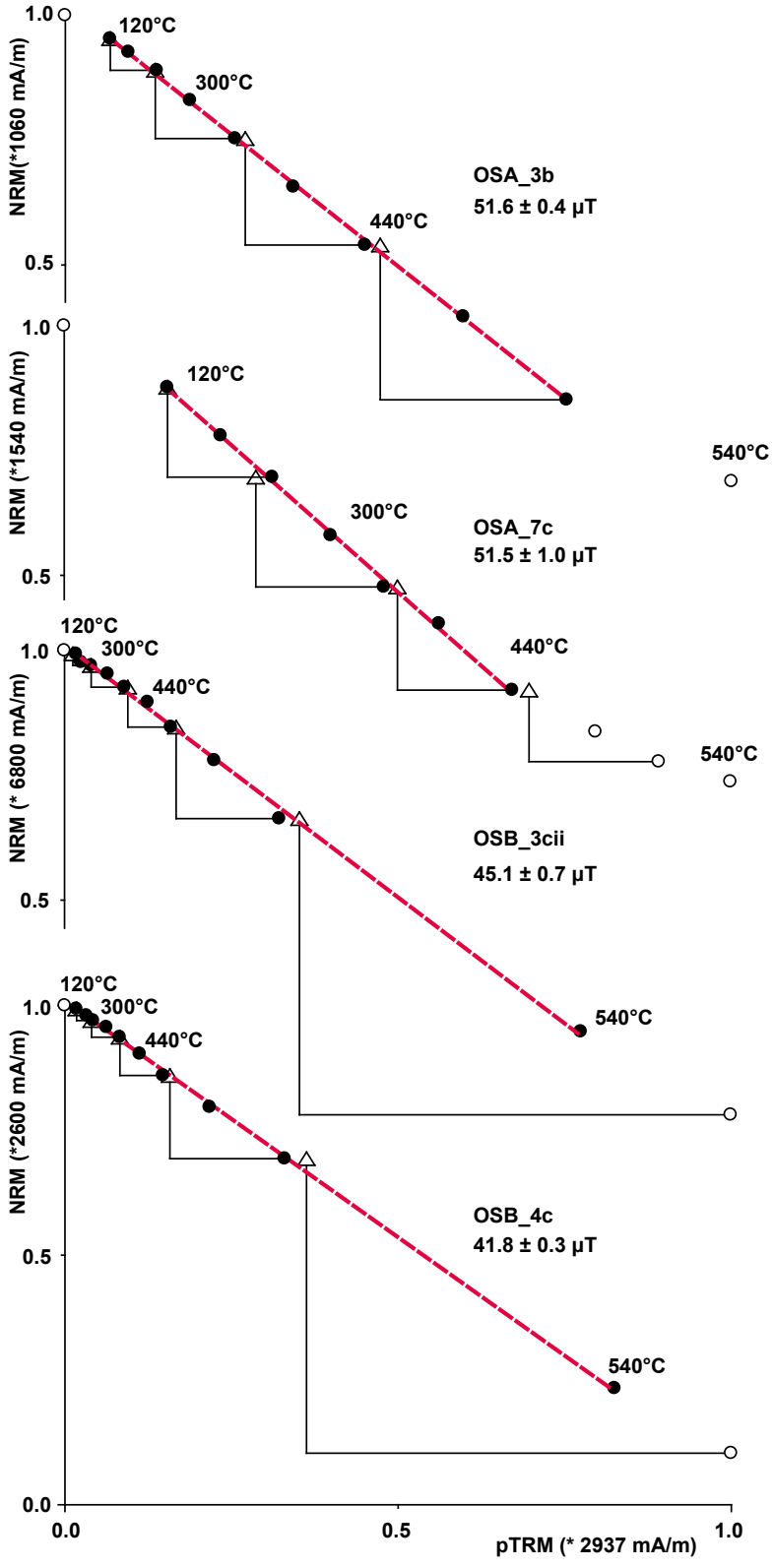
1.0
0.5
NRM(*1060 mA/m)
120°C
300°C
440°C
OSA_3b
51.6 ± 0.4 µT
NRM (*1540 mA/m)
120°C
300°C
440°C
540°C
OSA_7c
51.5 ± 1.0 µT
NRM (* 6800 mA/m)
120°C
300°C
440°C
540°C
OSB_3cii
45.1 ± 0.7 µT
NRM (*2600 mA/m)
120°C
300°C
440°C
540°C
OSB_4c
41.8 ± 0.3 µT
0.0
0.5
1.0
pTRM (* 2937 mA/m)

Fig. 9

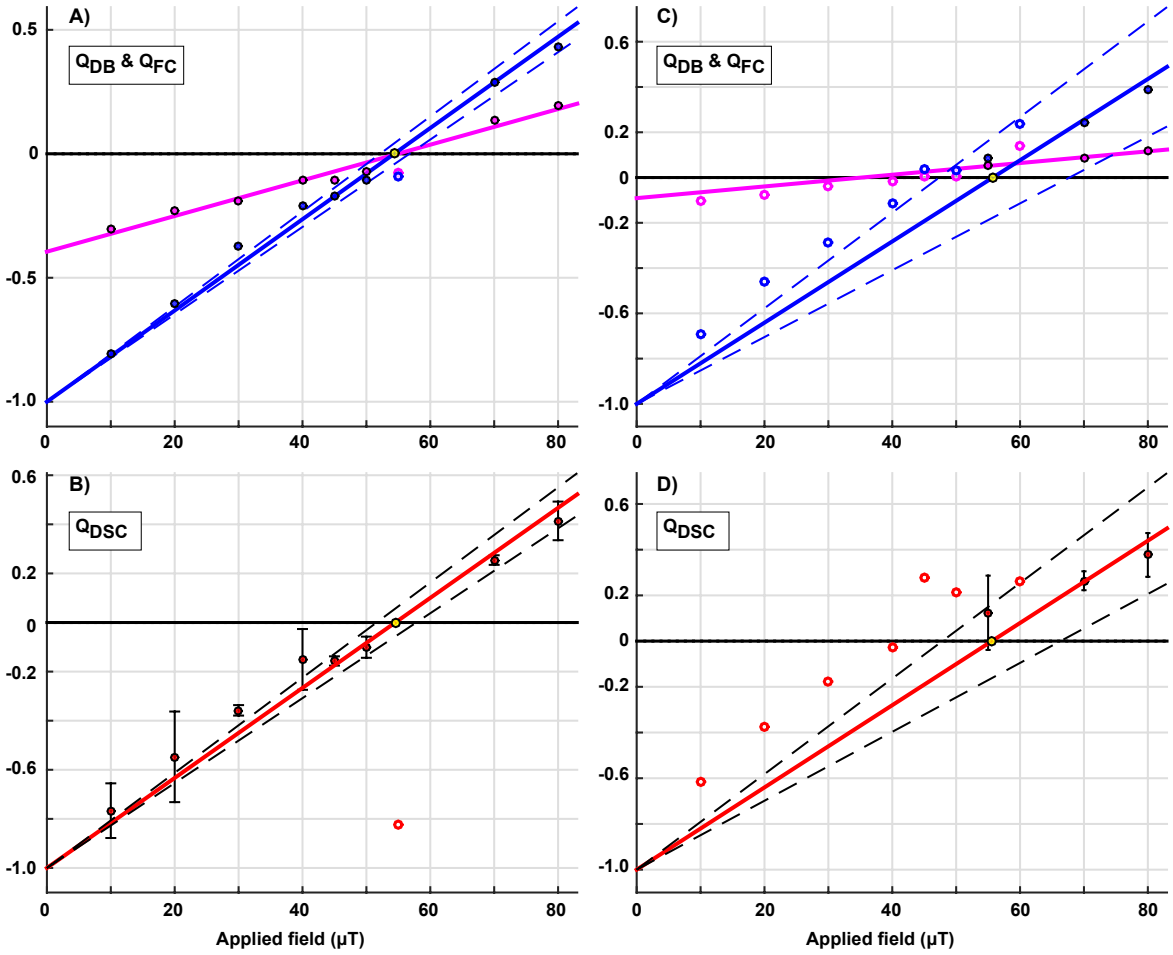
A)
$Q_{DB}$ & $Q_{FC}$
B)
$Q_{DSC}$
C)
$Q_{DB}$ & $Q_{FC}$
D)
$Q_{DSC}$
Applied field (μT)
Applied field (μT)

Fig. 10

729

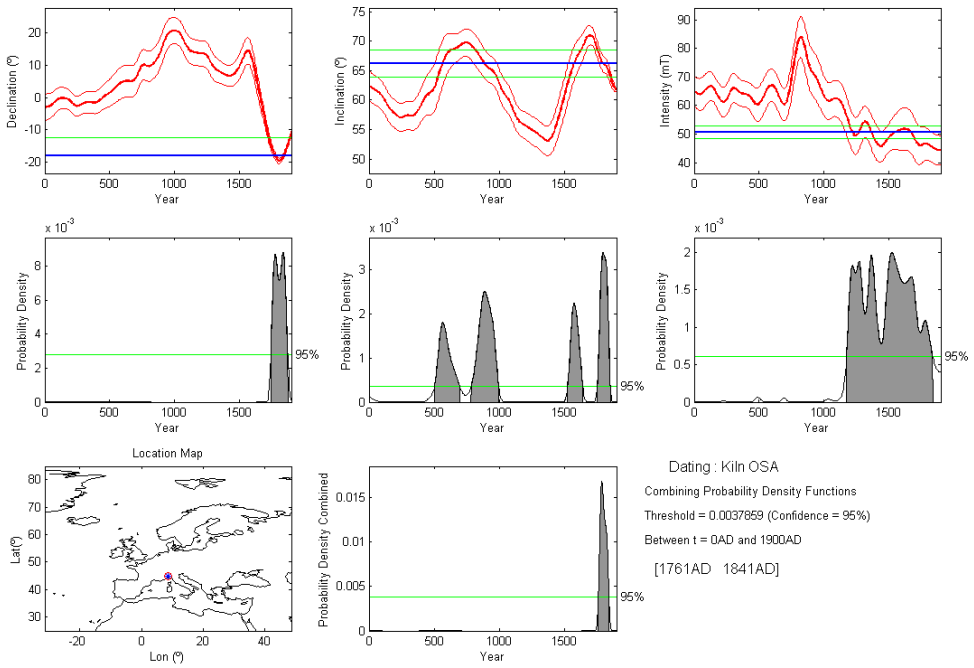


730

731 (a)

732

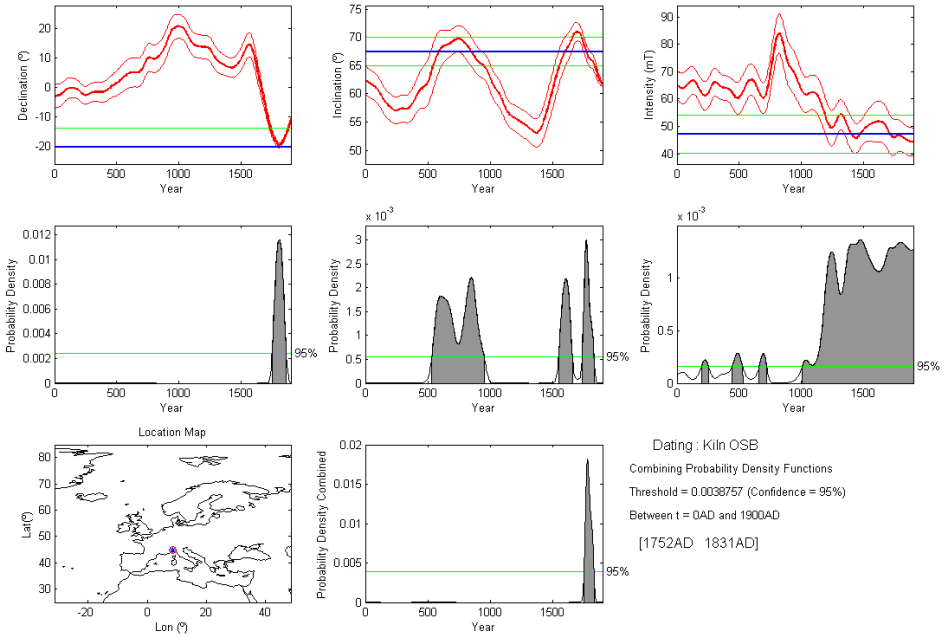


733

734 (b)

735 Fig. 11

736

737

738

| Sample | Temperature interval (°C) | D (°) | I (°) | MAD |
|---|---|---|---|---|
| **Kiln OSA:** | | | | |
| OSA-1a | 180-580 | 334.5 | 64.2 | 1.5 |
| OSA-2a | 180-580 | 354.0 | 68.5 | 1.3 |
| OSA-3a | 220-580 | 335.4 | 68.4 | 0.9 |
| OSA-4a | 140-580 | 354.9 | 68.5 | 1.3 |
| OSA-5a | 140-540 | 354.2 | 67.3 | 1.7 |
| OSA-6a | 220-580 | 341.7 | 63.8 | 1.2 |
| OSA-7a | 100-580 | 329.6 | 64.1 | 2.1 |
| OSA-9a | 260-580 | 334.3 | 64.2 | 1.1 |
| OSA-10a | 140-580 | 345.5 | 66.5 | 1.7 |
| OSA-12a | 140-580 | 336.9 | 64.2 | 1.6 |
| OSA-14a | 260-580 | 344.3 | 65.8 | 1.5 |
| ***Mean value:*** | | | | |
| N=11 | $D_m$= 341.8° | $I_m$= 66.2° | k=389 | $\alpha_{95}$= 2.3° |
| | | | | |
| **Kiln OSB:** | | | | |
| OSB-1a | 100-580 | 329.3 | 69.7 | 1.8 |
| OSB-2a | 140-580 | 349.3 | 70.7 | 1.2 |
| OSB-3a | 180-580 | 340.8 | 70.8 | 1.3 |
| OSB-4a | 380-580 | 342.2 | 63.3 | 1.1 |
| OSB-5a | 180-580 | 339.2 | 66.4 | 1.2 |
| OSB-6a | 260-580 | 342.5 | 64.8 | 1.6 |
| OSB-7a | 140-580 | 335.7 | 68.5 | 1.3 |
| OSB-8a | 140-580 | 337.9 | 64.9 | 1.0 |
| ***Mean value:*** | | | | |
| N=8 | $D_m$= 339.6° | $I_m$= 67.5° | k=504 | $\alpha_{95}$= 2.5° |

739

740

741 Table 1

742

743

744

| Sample | n | Tmin | - | Tmax | f | g | q | Drat | H | Fatrm | Hatrm | Fcr | Hatrm,cr |
|---|---|---|---|---|---|---|---|---|---|---|---|---|---|
| *Kiln OSA* | | | | | | | | | | | | | |
| OSA_1b | 9 | 120 | - | 510 | 0,57 | 0,86 | 38,2 | 1,1 | 53,9 ± 0,7 | 0,988 | 53,2 ± 0,7 | 0,992 | 53,2 ± 0,7 |
| OSA_1c | 9 | 120 | - | 510 | 0,69 | 0,87 | 56,2 | 2,4 | 55,1 ± 0,6 | 0,992 | 54,7 ± 0,6 | 1,005 | 54,4 ± 0,6 |
| OSA_2b | 9 | 120 | - | 510 | 0,69 | 0,87 | 51,3 | 1,9 | 53,5 ± 0,6 | 0,946 | 50,7 ± 0,6 | 1,046 | 48,4 ± 0,6 |
| OSA_2c | 9 | 120 | - | 510 | 0,68 | 0,87 | 36,5 | 1,7 | 51,3 ± 0,8 | 0,991 | 50,9 ± 0,8 | 1,040 | 48,9 ± 0,8 |
| OSA_3b | 9 | 120 | - | 510 | 0,71 | 0,84 | 81,2 | 2,4 | 51,6 ± 0,4 | 0,985 | 50,9 ± 0,4 | 0,984 | 50,9 ± 0,4 |
| OSA_3c | 7 | 180 | - | 480 | 0,55 | 0,82 | 24,1 | 4,4 | 49,1 ± 0,9 | 0,995 | 48,9 ± 0,9 | 1,037 | 47,2 ± 0,9 |
| OSA_4b | 10 | 180 | - | 560 | 0,74 | 0,88 | 51,2 | 0,7 | 57,4 ± 0,7 | 0,974 | 55,9 ± 0,7 | 1,039 | 53,8 ± 0,7 |
| OSA_4c | 10 | 180 | - | 560 | 0,74 | 0,88 | 74,9 | 1,8 | 53,6 ± 0,5 | 1,006 | 53,9 ± 0,5 | 1,042 | 51,7 ± 0,4 |
| OSA_5b | 9 | 240 | - | 560 | 0,94 | 0,78 | 49,3 | 3,0 | 44,7 ± 0,7 | 1,052 | 47,0 ± 0,7 | 0,999 | 47,0 ± 0,7 |
| OSA_5c | 10 | 180 | - | 560 | 0,95 | 0,81 | 65,3 | 2,4 | 49,1 ± 0,6 | 0,981 | 48,2 ± 0,6 | 1,003 | 48,1 ± 0,6 |
| OSA_6b | 7 | 120 | - | 440 | 0,59 | 0,83 | 30,6 | 3,3 | 52,8 ± 0,9 | 0,989 | 52,2 ± 0,8 | 1,034 | 50,5 ± 0,8 |
| OSA_6c | 7 | 120 | - | 440 | 0,51 | 0,83 | 20,9 | 4,0 | 52,0 ± 1,1 | 1,003 | 52,1 ± 1,1 | 1,022 | 51,0 ± 1,0 |
| OSA_7b | 7 | 120 | - | 440 | 0,51 | 0,83 | 20,8 | 3,5 | 52,2 ± 1,1 | 0,986 | 51,5 ± 1,0 | 1,029 | 50,0 ± 1,0 |
| OSA_7c | 7 | 120 | - | 440 | 0,58 | 0,83 | 24,5 | 3,4 | 51,5 ± 1,0 | 1,006 | 51,7 ± 1,0 | 1,038 | 49,8 ± 1,0 |
| OSA_7d | 7 | 120 | - | 440 | 0,53 | 0,82 | 13,8 | 2,1 | 55,5 ± 1,7 | 0,992 | 55,1 ± 1,7 | 1,071 | 51,4 ± 1,6 |
| OSA_9b | 9 | 120 | - | 510 | 0,80 | 0,86 | 38,5 | 2,6 | 50,8 ± 0,9 | 0,966 | 49,1 ± 0,9 | 1,032 | 47,6 ± 0,9 |
| OSA_9c | 6 | 180 | - | 440 | 0,60 | 0,78 | 21,7 | 1,1 | 54,4 ± 1,2 | 1,002 | 54,5 ± 1,2 | 1,084 | 50,2 ± 1,1 |
| OSA_10b | 6 | 180 | - | 440 | 0,51 | 0,80 | 10,7 | 1,0 | 55,7 ± 2,1 | 1,010 | 56,3 ± 2,1 | 1,063 | 52,9 ± 2,0 |
| OSA_10c | 7 | 180 | - | 480 | 0,65 | 0,82 | 17,7 | 2,7 | 55,0 ± 1,7 | 1,021 | 56,1 ± 1,7 | 1,051 | 53,4 ± 1,6 |
| OSA_11b | 8 | 120 | - | 480 | 0,66 | 0,85 | 20,0 | 5,3 | 51,4 ± 1,4 | 1,019 | 52,3 ± 1,5 | 1,027 | 51,0 ± 1,4 |
| OSA_11bii | 8 | 120 | - | 480 | 0,69 | 0,85 | 19,5 | 2,6 | 49,0 ± 1,5 | 1,072 | 52,5 ± 1,6 | 1,034 | 50,7 ± 1,5 |
| OSA_13b | 9 | 120 | - | 510 | 0,70 | 0,87 | 25,8 | 2,5 | 49,2 ± 1,2 | 1,008 | 49,6 ± 1,2 | 1,019 | 48,6 ± 1,1 |
| OSA_13c | 10 | 120 | - | 540 | 0,78 | 0,89 | 37,8 | 1,9 | 49,8 ± 0,9 | 1,059 | 52,8 ± 1,0 | 1,017 | 51,9 ± 1,0 |
| | | | | | **Unweighted average** | | | | 52,1 ± 2,9 | | 52,2 ± 2,6 | | **50,6 ± 2,2** |
| *Kiln OSB* | | | | | | | | | | | | | |
| OSB-3cii | 10 | 120 | - | 540 | 0,75 | 0,63 | 29,7 | 3,0 | 45,1 ± 0,7 | 1,012 | 45,6 ± 0,7 | 1,013 | 45,0 ± 0,7 |
| OSB-4b | 9 | 240 | - | 560 | 0,86 | 0,62 | 83,5 | 2,1 | 40,5 ± 0,3 | 1,000 | 40,5 ± 0,3 | 1,011 | 40,1 ± 0,3 |
| OSB-4c | 10 | 120 | - | 540 | 0,76 | 0,60 | 58,4 | 3,2 | 41,8 ± 0,3 | 0,990 | 41,4 ± 0,3 | 1,030 | 40,2 ± 0,3 |
| OSB-4cii | 10 | 120 | - | 540 | 0,75 | 0,61 | 65,5 | 3,3 | 45,4 ± 0,3 | 0,989 | 44,9 ± 0,3 | 1,033 | 43,5 ± 0,3 |
| OSB-5b | 10 | 120 | - | 540 | 0,74 | 0,88 | 19,5 | 2,2 | 62,9 ± 2,1 | 0,982 | 61,8 ± 2,1 | 1,004 | 61,6 ± 2,1 |
| OSB-5c | 8 | 120 | - | 480 | 0,73 | 0,85 | 22,4 | 2,8 | 60,7 ± 1,7 | 0,967 | 58,7 ± 1,6 | 1,025 | 57,3 ± 1,6 |
| OSB-6b | 10 | 120 | - | 540 | 0,77 | 0,88 | 45,2 | 3,0 | 47,3 ± 0,7 | 0,983 | 46,5 ± 0,7 | 1,007 | 46,2 ± 0,7 |
| OSB-6c | 7 | 20 | - | 400 | 0,59 | 0,83 | 20,1 | 4,6 | 45,2 ± 1,1 | 0,994 | 44,9 ± 1,1 | 1,032 | 43,5 ± 1,1 |
| OSB-6d | 9 | 120 | - | 510 | 0,70 | 0,87 | 33,7 | 1,9 | 46,7 ± 0,9 | 0,987 | 46,1 ± 0,8 | 1,010 | 45,6 ± 0,8 |
| OSB-7b | 9 | 120 | - | 510 | 0,50 | 0,81 | 22,0 | 2,3 | 53,3 ± 1,0 | 0,994 | 53,0 ± 1,0 | 1,035 | 51,2 ± 0,9 |
| OSB-8aii | 10 | 20 | - | 510 | 0,54 | 0,83 | 12,9 | 4,2 | 45,2 ± 1,6 | 0,989 | 44,7 ± 1,6 | 1,020 | 43,8 ± 1,5 |
| | | | | | **Unweighted average** | | | | 48,6 ± 7,3 | | 48,0 ± 6,9 | | **47,1 6,9** |

745

746

747 Table 2

748

749

| Method | PI (μT) | 95% conf. | n/N | R-squared | RMSE |
|---|---|---|---|---|---|
| ***Kiln OSA*** | | | | | |
| MSP-DB | 54.9 | [51.1 - 59.4] | 8/10 | 0.9739 | 0.0301 |
| MSP-FC | 54.3 | [52.2 - 56.7] | 8/10 | 0.9882 | 0.0450 |
| MSP-DSC (α = 0.5) | 54.5 | [51.6 - 57.8] | 8/10 | 0.9584 | 0.3283 |
| MSP-DSC (α = 0.2) | 54.6 | [52.5 - 56.8] | 8/10 | 0.9825 | 0.2435 |
| MSP-DSC (α = 0.8) | 54.8 | [51.0 - 59.0] | 8/10 | 0.9234 | 0.3941 |
| Preferred PI for OSA: | **54.5 ± 3.5 μT** | | | | |
| ***Kiln OSB*** | | | | | |
| MSP-DB | 35.2 | n.d. | 3/10 | 0.9747 | 0.0074 |
| MSP-FC | 55.7 | [47.4 - 67.7] | 3/10 | 0.6558 | 0.0884 |
| MSP-DSC (α = 0.5) | 55.6 | [47.8 - 66.3] | 3/10 | 0.2559 | 0.3059 |
| MSP-DSC (α = 0.2) | 56.0 | [49.0 - 65.3] | 3/10 | 0.5589 | 0.2968 |
| MSP-DSC (α = 0.8) | 55.2 | [46.6 - 67.6] | 3/10 | -0.2662 | 0.3179 |
| Preferred PI for OSB: | **Not reliable** | | | | |

Table 3

**Appendix**

# Matlab code estimating the factor (f) for ATRM correction during Thellier-Thellier

by Pierre CAMPS, CNRS and University of Montpellier, France. pcamps [at] univ-montp2 [dot] fr

`v1.0 (01/01/2015)`

# Contents



# Preliminary comments

First, we compute the A-TRM tensor by means of procedures adapted from L. Tauxe's algorithm implemented by the fortran program aarm_s **[Tauxe, 1998]** that use the off-axis remanence terms.

Then, we calculate anisotropy factor correction following the method described by **Veitch et al., 1984** (Arch. Sc. Geneve, 37, 3 pp 359-373).

INPUT file : JRA format with 6 measurements in the following order +Z, -Z, +X, -X, +Y, -Y (example of an input file is provided at the end of this document)

OUTPUT : f_atrm factor and some others parameters...

**Cautionary notes** :

**[1]** In this program, the NRM direction in core coordinates is determined from the +Z and -Z steps at the temperature step selected for the anisotropy determination. If this direction is significantly different from the direction obtained by with PCA analysis processed within the temperature interval used for paleointensity estimate, this later should be used.

**[2]** This software is distributed on an "AS IS" basis, WITHOUT WARRANTY OF ANY KIND, either express or implied.

**[3]** Papers reporting results obtained with the present source code may cite in the references or bibliography the paper by Tema et al., Stud. Geophys. Geod., XX, (X), pp-pp, 2015.

# Set initial conditions.

```
input_filename='OS1_3b.jra';
nb_Pos = 6;
```

First, check the number of steps measured in the datafile (MUST be equal to 6)

```
infile = fopen(input_filename,'r');
 allText = textscan(infile,'%s','delimiter','\n','CommentStyle','%');
 numberOfLines = length(allText{1});
 frewind(infile);

 if numberOfLines ~= nb_Pos
     disp('ERROR : input file in wrong format !!!')
     disp('6 measurements +Z,-Z,+X,-X,+Y,-Y are required for
calculation')
     return;
 end
```

Preallocating memory for arrays

```
sample_name = cell(1,numberOfLines);
xyz = zeros(nb_Pos,3);      % cartesians coordinates
bline = zeros(3,3);         % NRM remaining.
H6 = zeros(nb_Pos,3);       % applied field directions
a6 = zeros(nb_Pos*3,nb_Pos);
w  = zeros(1,nb_Pos*3);
```

# Build the design matrix for 6-positions measurement scheme

```
dec6 = [0 pi/2 0 pi 3*pi/2 0];
inc6 = [0 0 pi/2 0 0 -pi/2];

for i=1:nb_Pos
  [H6(i,1),H6(i,2),H6(i,3)]= sph2cart(dec6(i),inc6(i),1.0);
end

% Fill nonzero components of design matrix
for i=1:nb_Pos
  index = (i-1)*3+1;
   a6(index,1) = H6(i,1);
   a6(index,4) = H6(i,2);
   a6(index,6) = H6(i,3);
  index = (i-1)*3+2;
   a6(index,4) = H6(i,1);
   a6(index,2) = H6(i,2);
   a6(index,5) = H6(i,3);
  index = (i-1)*3+3;
   a6(index,6) = H6(i,1);
   a6(index,5) = H6(i,2);
   a6(index,3) = H6(i,3);
end

b6 = (a6'*a6)\a6'; % design matrix
```

# Compute the pTRM acquired along +X,+Y+Z,-X,-Y,-Z

Read the data file

```
i=0;
while ~feof(infile)
   inline=fgetl(infile);
   if ~isempty(inline) && ~strncmp(inline,'%',1)
     i=i+1;
     A=sscanf(inline,'%6c, %5c, %f, %f, %f, %f ');
     sample_name{i} = strcat(A(1:6));
     treatment{i}   = strcat(A(7:11));
     xyz(i,1) = A(12) * 10^A(15);
     xyz(i,2) = A(13) * 10^A(15);
     xyz(i,3) = A(14) * 10^A(15);
   end
end
```

Compute the baselines (NRM remaining)

```
for i = 1:3
  bline(1,i) = (xyz(3,i) + xyz(4,i))/2; % +X and -X
  bline(2,i) = (xyz(5,i) + xyz(6,i))/2; % +Y and -Y
  bline(3,i) = (xyz(1,i) + xyz(2,i))/2; % +Z and -Z
end
```

Compute the pTRM acquired in the 6 positions

```
pTRM(1,:) = xyz(3,:) - bline(1,:); % +X
pTRM(2,:) = xyz(5,:) - bline(2,:); % +Y
pTRM(3,:) = xyz(1,:) - bline(3,:); % +Z
pTRM(4,:) = xyz(4,:) - bline(1,:); % -X
pTRM(5,:) = xyz(6,:) - bline(2,:); % -Y
pTRM(6,:) = xyz(2,:) - bline(3,:); % -Z
```

# Quality tests

Check possible changes in NRM directions during pTRM acquisitions

```
fprintf('NRM directions after acquisition along X, Y, and Z \n');
for i = 1:3

angle=atan2(norm(cross(bline(3,:),bline(i,:))),dot(bline(3,:),bline(i
,:)));
  [nrmDECL,nrmINC,nrmF] = cart2sph(bline(i,1),bline(i,2),bline(i,3));

  formatSpec = 'Decl: %6.1f  Inc : %6.1f Angle : % 6.1f \n';
  fprintf(formatSpec, rad2deg(nrmDECL), rad2deg(nrmINC),
rad2deg(angle));
end
NRM directions after acquisition along X, Y, and Z
Decl:   85.4  Inc :   65.0 Angle :    0.8
Decl:   82.3  Inc :   66.1 Angle :    1.2
Decl:   85.3  Inc :   65.8 Angle :    0.0
```

Compare the remanence direction to the direction of applied field

```
angle_threshold = 15;
for i = 1:nb_Pos
  angle=atan2(norm(cross(H6(i,:),pTRM(i,:))),dot(H6(i,:),pTRM(i,:)));
  if rad2deg(angle) > angle_threshold
```

```
      formatSpec = 'WARNING, angle between pTRM and applied field :
%4.1f for position : %d \n';
      fprintf(formatSpec, rad2deg(angle), i);
  else
      formatSpec = 'OK, angle between pTRM and applied field : %4.1f
for position : %d \n';
      fprintf(formatSpec, rad2deg(angle), i);
  end
end
OK, angle between pTRM and applied field :  1.6 for position : 1
OK, angle between pTRM and applied field :  0.3 for position : 2
OK, angle between pTRM and applied field :  1.7 for position : 3
OK, angle between pTRM and applied field :  1.6 for position : 4
OK, angle between pTRM and applied field :  0.3 for position : 5
OK, angle between pTRM and applied field :  1.7 for position : 6
```

# Calculate tensor and sigma value.

Tensor before normalization

```
for i=1:nb_Pos
  for j=1:3
    index = (i-1)*3+j;
    w(index) = pTRM(i,j);
  end
end

x = b6 * w';
a = diag([x(1) x(2) x(3)]);
a(1,2) = x(4);
a(1,3) = x(6);
a(2,3) = x(5);
a(2,1) = a(1,2);
a(3,2) = a(2,3);
a(3,1) = a(1,3);
```

Tensor normalized by trace

```
t=sum(diag(a));
a=a/t;
w=w/t;
```

Compute sigma value

```
comp = horzcat(reshape(a,1,9),reshape(-a,1,9));
S = sum((w - comp).^2);

free = 12; % npos*3-6
if(S > 0)
       sigma=sqrt(S/free);
else
       sigma=0.;
end
```

Calculate eigenvalues and right eigenvectors of the A-TRM tensor

```
[eigenVectors,eigenValues] = eig(a,'vector');
for i=1:3
```

```
[decl_ev,incl_ev,F_ev]=cart2sph(eigenVectors(1,i),eigenVectors(2,i),e
igenVectors(3,i));

  decl_ev=rad2deg(decl_ev);
  incl_ev=rad2deg(incl_ev);
  if incl_ev < 0
        incl_ev=-incl_ev;
        decl_ev=decl_ev-180;
  end
  if decl_ev < 0
        decl_ev=decl_ev+360;
  end

  formatSpec = 'Sample %s   eing_v %4.6f   Decl : %3.1f   Incl :
%3.1f \n';
  fprintf(formatSpec, sample_name{1},
eigenValues(i),decl_ev,incl_ev);
end
Sample OS1_3b   eing_v 0.311277   Decl : 351.1   Incl : 72.3
Sample OS1_3b   eing_v 0.342807   Decl : 219.9   Incl : 11.9
Sample OS1_3b   eing_v 0.345916   Decl : 127.1   Incl : 12.9
```

# Correction Factor for TRM anisotroptry

Please note that NRM direction is obtained from the +Z and -Z steps. This direction **must** be taken from the Arai plot if it's significantly different.

```
m = bline(3,:)'; % NRM direction

u=[0;0;1]; % u is the unit vector along z-axis
```

Calculate the unit vector (h) in direction of ancient field

```
h_anc=a\m/norm(a\m);

[rDec_c,rInc_c,r]=cart2sph(h_anc(1),h_anc(2),h_anc(3));
Dec_c=radtodeg(rDec_c);
if Dec_c < 0
       Dec_c = 360.0 + Dec_c;
end
Inc_c=radtodeg(rInc_c);

angle_r=atan2(norm(cross(m,h_anc)),dot(m,h_anc));
angle=rad2deg(angle_r);
```

Calculate the correction factor f

```
f=norm(a*u)/norm(a*h_anc);
```

Calculate the degree of Anisotropie (Nagata, T., 1961. Rock Magnetism, 2nd edition. Maruzen, Tokyo)

```
P = max(diag(a))/min(diag(a));
```

Calculate the shape parameter (Jelinek, V., 1981. Tectonophysics 79, T63?T67.)

```
shape_T = (2*log(a(2,2))- log(a(1,1)) -log(a(3,3))) /
(log(max(diag(a))) - log(min(diag(a))));
```

# Print the result

```
fprintf(' Sample    f        P       T      Dec     Inc     Dec_c
Inc_c   Angle  \n');
fprintf('-------------------------------------------------------------
------------ \n');

formatSpec = ' %s %7.4f  %6.3f  %6.3f %7.1f %7.1f %7.1f %7.1f
%7.1f\n';
fprintf(formatSpec,sample_name{1}, f, P, shape_T, rad2deg(nrmDECL),
rad2deg(nrmINC), Dec_c, Inc_c, angle);
 Sample    f        P       T      Dec     Inc     Dec_c   Inc_c
Angle
-------------------------------------------------------------------
---
 OS1_3b  0.9851   1.096   1.114    85.3    65.8    81.1    67.8
2.6
```

# Example of INPUT file

```
type OS1_3b.jra
% Name, treat,   Xc,    Yc,    Zc,   power
OS1_3b, Z+440,  0.05,  2.34,  9.97,  -1
OS1_3b, Z-440,  0.33,  2.26,  0.31,  -1
OS1_3b, X+440,  5.43,  2.33,  4.89,  -1
OS1_3b, X-440, -5.05,  2.36,  5.19,  -1
OS1_3b, Y+440,  0.28,  7.49,  5.02,  -1
OS1_3b, Y-440,  0.31, -3.10,  4.98,  -1
```

Published with MATLAB® R2014b